Supplementary Notes:

1. Simulated magnetic field pattern

To model the magnetic field pattern from MNP-labeled cells to be imaged with the quantum diamond microscope, we approximated a labeled cell as a spherical shell of uniformly magnetized material. Such a shell can be expressed as the superposition of two uniform spheres of opposite magnetizations, M and $-M$, with radii equal to the inner and outer radius of the spherical shell, respectively. The magnetic field outside of a uniformly magnetized sphere of radius R is described by the magnetic vector potential A, in spherical coordinates and SI units, as[1]

$$\vec{A}(\vec{r}) = \frac{\mu_0 M R^3}{3r^2} \sin\theta \, \hat{\varphi} \tag{1}$$

where μ_0 is the permeability of free space. The resulting magnetic field is

$$\vec{B} = \vec{\nabla} \times \vec{A} = \frac{\mu_0 M R^3}{3} \left[\frac{3(\hat{M}\cdot\hat{r})\hat{r} - \hat{M}}{r^3} \right] \tag{2}$$

This result is simply the dipole field produced by magnetic dipole moment $m = (4\pi MR^3)/3 = MV$, where V is the sphere's volume, which is equivalent to the case of all magnetic material concentrated at the sphere's center. Therefore, the superposition of two oppositely-magnetized spheres, and hence the case of the spherical shell, is also equivalent to a dipole field with $m = M\delta V$, where δV is the shell's volume. It is thus sufficient to model a uniformly-labeled cell as a point dipole located at the cell's center, with $m = N \times m_{MNP}$ for N particles each with magnetic moment m_{MNP}.

The quantity measured by the quantum diamond microscope is $B_{||}$, the projection of the magnetic field given by (2) onto the NV axis, which is parallel to both the applied bias magnetic field B_0 and the MNP-labeled cell's magnetization vector:

$$B_{||} = \vec{B} \cdot \hat{M} = \frac{\mu_0 m}{4\pi} \left(\frac{3(\hat{m}\cdot\hat{r})^2 - 1}{r^3} \right). \tag{3}$$

This quantity is evaluated (**Fig. S1**) in the horizontal plane of the NV-diamond sensor surface using the following parameters: N = 10,000 MNPs with $m_{MNP} = 8.6 \times 10^{-16}$ emu (for the 20-nm core magnetite MNP used here, under a 400 G magnetizing field B_0) uniformly distributed on a 15-μm diameter spherical cell in contact with the diamond surface. The magnetization vector is oriented at an angle of $90° - \vartheta_t/2 \approx 35.3°$ with respect to the diamond surface, where $\vartheta_t = \cos^{-1}(-1/3)$ is the tetrahedral angle between the diamond crystal axes.

Nature Methods: doi:10.1038/nmeth.3449

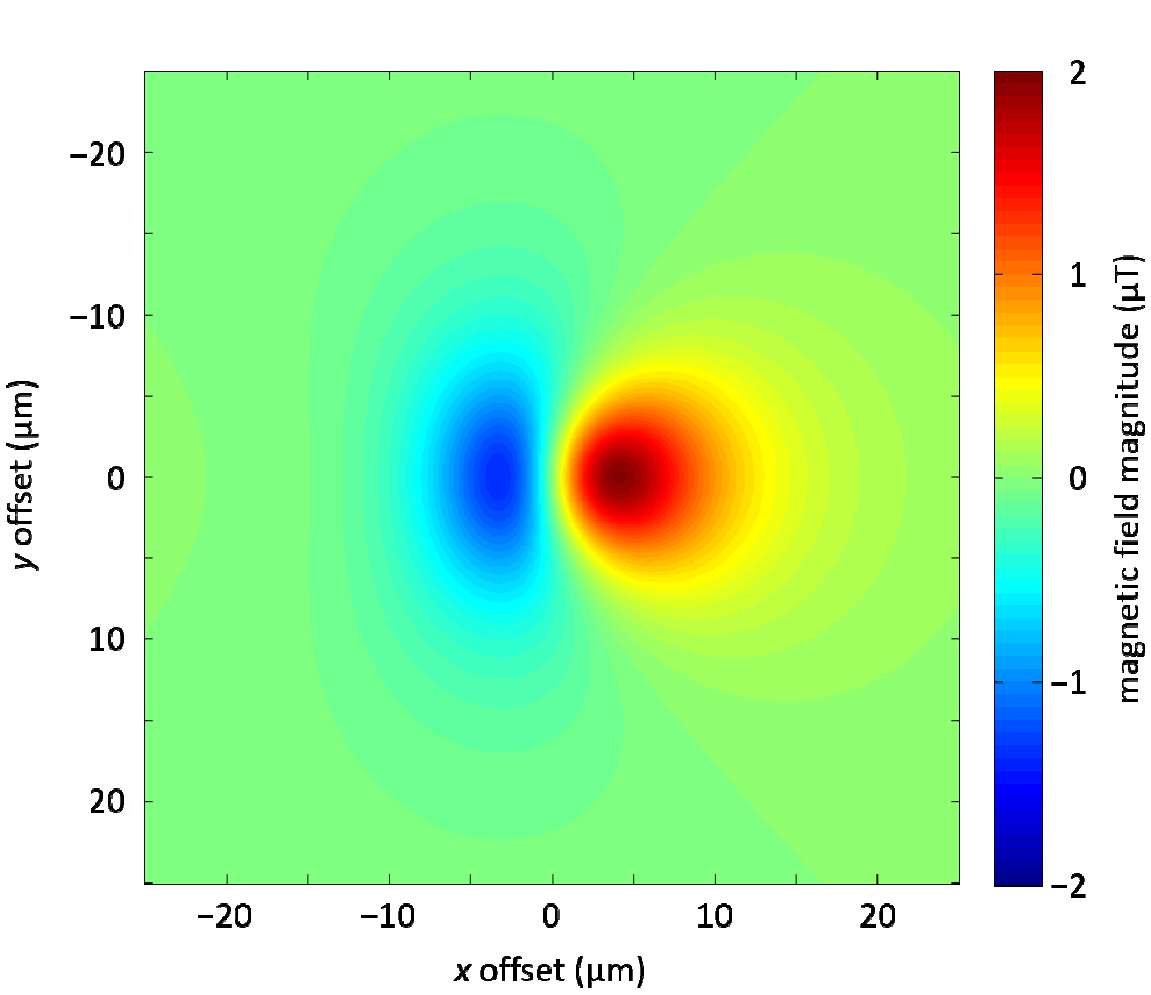


Figure S1: Simulated magnetic field pattern observed from a MNP-labeled cell located a distance of 7.5 μm from the diamond surface (in the *z*-direction, out of the page). The cell has been modeled as a uniformly-magnetized spherical shell.

2. Distinguishing Adjacent Cells

Magnetically labeled cells produce magnetic fields that extend to many times the size of each cell, and therefore images of closely-spaced cells may show overlapping signals (**Fig. S2**). Such overlap, however, does not degrade the ability to quantify biomarker expression of adjacent or contacted cells. The superparamagnetic nanoparticles bound to each cell's surface align with the applied bias magnetic field B_0 to create a characteristic 2-lobed shape common to all labeled cells (**Fig. S1**). Since the cellular magnetic field is much weaker than the bias field, the magnetic signals from different cells do not interact. The total field from many closely-spaced cells can thus be modeled as a superposition of individual fields of the form given above (Equation 3). This allows us to fit the total field of several adjacent or contacted cells (**Fig. S2**). Each cell's magnetic signal can be easily and separately distinguished. The magnetic imaging data shown in the main text was analyzed using a superposition model to fit to groups of contiguous cells.

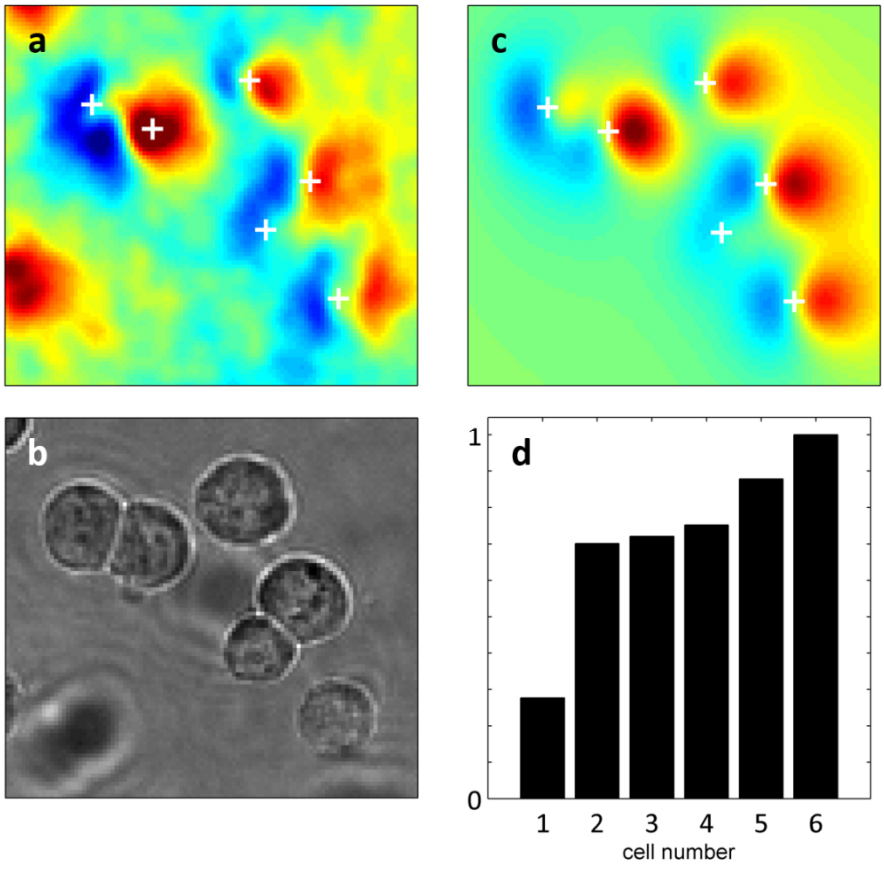


Figure S2: (a) Example of MNP-labeled cells producing overlapping magnetic patterns in images from the quantum diamond microscope. White crosses mark the centers of six cells. Color scale is ±5 μT. **(b)** Spatially co-registered bright-field image. (**c**) Magnetic field pattern resulting from a fit of the magnetic image in **a** to a superposition of cellular fields, each given by the analytic expression of Equation 3. **(d)** Bar chart showing relative magnetic signal strengths for the six cells obtained from the fit shown in **c**. The measurement error is approximately 2% of the largest signal shown here, allowing for discrimination between the six signal magnitudes.

3. Quantum Diamond Microscope Resolution

For applications requiring sub-cellular discrimination of magnetic labels, the spatial resolution of the quantum diamond microscope is set by a combination of: (i) the resolution of the optical detection system, and (ii) the characteristic distance between the dipolar magnetic labels and the ~10-nm thick NV probe layer at the diamond surface. When magnetic labels are brought within <500 nm of the surface, the spatial imaging resolution is limited primarily by optical diffraction, and sub-cellular features can easily be discerned[2]. Furthermore, we have shown elsewhere that optical super-resolution techniques[3] or Fourier imaging methods can enable sub-diffraction magnetic imaging using NV centers with resolution down to ~10 nm, assuming the magnetic labels are sufficiently close to the diamond surface.

For the investigations described in the main text, we operated the quantum diamond microscope with a coarse transverse imaging resolution of 4.7 μm, which was well-matched to the spatial extent of the target magnetic field patterns from cells labeled with magnetic nanoparticles (MNPs). Substituting a different objective or tube lens into the microscope readily yields a diffraction-limited resolution of about 450 nm for imaging sub-cellular features. The ability to vary straightforwardly the magnetic imaging resolution down to (or even below) the optical diffraction limit is an important advantage of the quantum diamond microscope, compared to other magnetic imaging technologies, e.g., enabling the imaging of magnetic fields produced by individual MNPs (**Fig. S3**).

We note that, as usual for fluorescence-based techniques, an increase in magnification leads to a corresponding reduction in the light collected per detector pixel (for fixed optical excitation intensity); to compensate, either the signal acquisition time must be increased, or the field of view decreased to enable greater optical excitation intensity. On the other hand, sensitivity to magnetic sources in close proximity to the sensor is greatly enhanced by using higher magnification due to the r^{-3} scaling of dipolar magnetic fields at distance r from the source.

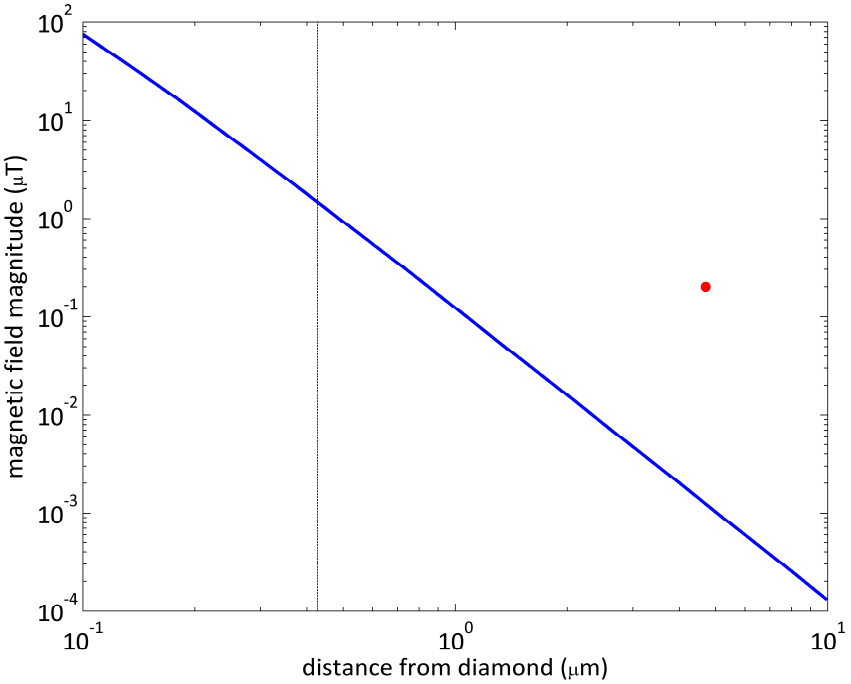


Figure S3: Calculated magnetic field magnitude (solid blue line) produced by a single fully-polarized magnetic nanoparticle (MNP) of the type used in this work (20-nm magnetite core with $m = 8.6 \times 10^{-16}$ emu). The vertical black line is the optical diffraction limit for 700-nm light (the approximate center of the NV^- emission spectrum) using a numerical aperture of 1. The red point gives the quantum diamond microscope's noise floor and imaging resolution (4.7 μm) for detecting cellular magnetic signals, as configured for the results presented in the main text. Diffraction-limited imaging can be straightforwardly achieved by using a higher-resolution objective. This could allow detection of single MNPs in a modified instrument.

4. Detecting Labeled Cancer Cells in Whole Blood

A key advantage of magnetic detection of rare cells over direct fluorescence detection is that magnetic fields penetrate complex and heterogeneous media such as whole blood; whereas optical signals from flow cytometry and comparable techniques are greatly degraded in all but the thinnest samples by absorption, scattering, and fluorescence from overlapping emitters. To demonstrate this advantage, we applied the quantum diamond microscope to magnetically tagged MCF7 cells (with EpCAM-specific MNP labels) spiked into human blood. In this sample, abundant erythrocytes obscure optical detection of the cancer cell, even for a relatively thin (~30 µm) layer of blood between the diamond surface and a glass coverslip (**Fig. S4**). However, the SNR of the magnetic field image shows no degradation, obtained under standard imaging conditions), such that the target cell can be readily detected. With straightforward alterations to the apparatus, this approach can be extended to magnetic detection of rare cells through an arbitrarily thick layer of blood or other opaque or fluorescent material.

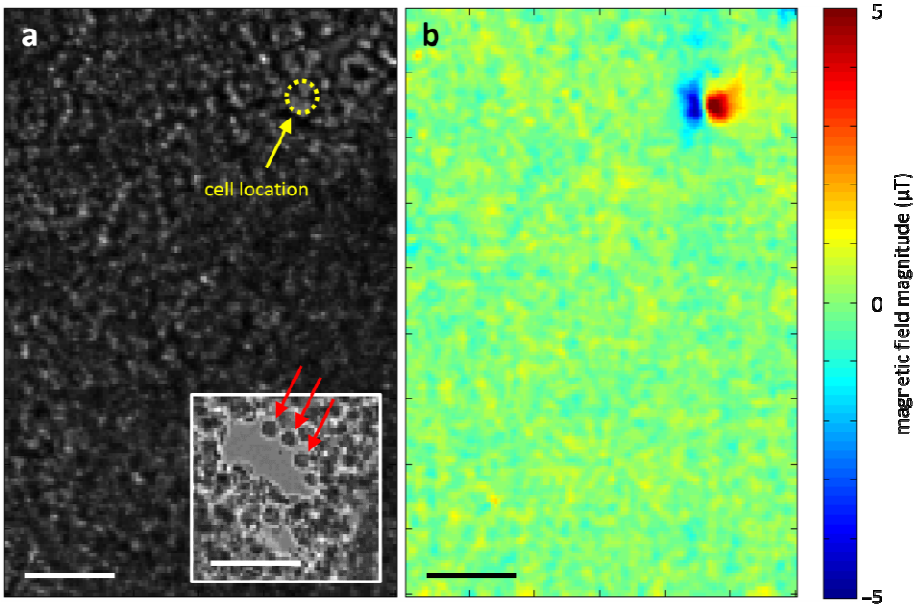


Figure S4: Rare cell magnetic detection in whole blood. **a.** Monochromatic bright-field transmission image showing a sample of human blood, with a single MNP-labeled SKBR3 cell present in the field of view (yellow dashed circle). The dense layer of erythrocytes impedes optical detection of the cancer cell. The inset shows a different field of view in which individual erythrocytes (marked with red arrows) can be identified near a gap in the dense layer. **b.** Magnetic image of the same field of view shown in **a**, clearly revealing the location of the MNP-tagged cell despite the presence of many background cells. Sample autofluorescence and scattering do not noticeably degrade the magnetic image. Scale bars 50 µm.

Method for Blood sample preparation: Samples were prepared by spiking SKBR3 cells into human whole blood. The cancer cells were targeted with MNPs and stained with CFSE using the procedure as described above. MNP-targeted and CFSE-stained SKBR3 cells were fixed and mixed with whole-blood samples. Whole-blood samples (3 mL) were taken from a healthy donor under approval of the Institutional Review Board (IRB) at the Massachusetts General Hospital.

5. Projected Improvements for Detection Apparatus

There are several ways in which the quantum diamond microscope described here could be improved for more sensitive and rapid imaging of magnetically-labeled targets. We identify three specific improvements that could be implemented with demonstrated technology:

1. increased number of NV centers in the diamond imaging sensor;
2. optimized microwave frequencies for detecting NV magnetic resonance; and
3. enhanced magnetic labeling for larger signals.

The first improvement, increasing the number of NV centers in the diamond sensor, has two aspects: a thicker NV sensing layer at the diamond chip surface as well as a higher NV density in the sensing layer. The current imaging sensor was created by implanting 14-keV $^{14}N^{+}$ ions at a dose of 5×10^{12} cm^{-2}. A calculation using Stopping and Range of Ions in Matter (SRIM) software predicts that such implantation forms an N-rich layer approximately 10 nm thick at a mean depth of ~20 nm below the surface. Following implantation, the diamond is annealed at high temperature to mobilize lattice vacancies, which bind to the implanted N defects to form NV centers.

For an improved imaging sensor, this shallow, thin (~10 nm) layer of NV centers could be increased to a thickness of 1 micron at a constant nitrogen density. Since the NV spin resonance line width is determined primarily by residual nitrogen impurities, maintaining this density would ensure that each NV center's magnetic field sensitivity is unchanged. Such a 1-micron thick NV sensing layer can be created by selectively incorporating nitrogen into the chemical vapor deposition (CVD) growth process, a demonstrated process called delta doping[4]. It is further possible to increase greatly the N-to-NV conversion ratio, which we estimate is limited in the current sensor to be less than 6%. Conversion efficiencies exceeding 30% have been demonstrated by introducing more vacancies into the lattice via electron or ion irradiation[5,6]. We therefore estimate that it would be straightforward to engineer a 1-micron thick sensing layer at the diamond surface with 300 times more NV centers to yield a corresponding increase in NV fluorescence rate and hence magnetic field sensitivity.

We stress that this thicker sensing layer would not significantly degrade the magnetic imaging resolution for MNP-labeled cells. While the spatial resolution of magnetic imaging is limited to approximately the sensing layer thickness, the magnetic field patterns produced by labeled cells have features larger than 1-micron. Likewise, the slight increase in mean distance from an NV center to the cell (about half a micron) is negligible for cells larger than several microns.

The second improvement, using optimized microwave frequencies, can be implemented after modest improvement of the spatial homogeneity ('flatness') of the bias magnetic field (B_0). By only probing NV centers at microwave frequencies corresponding to the points of maximum slope in the optically detected magnetic resonance (ODMR) spectrum, the magnetic field sensitivity is maximized. Currently, the 40-mT bias magnetic field — produced by a pair of permanent magnets — varies by approximately 40 μT over the 1-mm FOV, which corresponds to a shift in the NV spin resonance of greater than one line width. It is therefore not feasible to choose a single frequency that is optimal for all NV centers.

However, it would become feasible to do so if the bias field were made an order of magnitude flatter (more homogeneous), which could be realized with several additional small compensation magnets. Numerical simulation shows that this modification would improve the magnetic field sensitivity by a factor of about 2.5.

Finally, the third improvement, larger signals through enhanced magnetic labeling, has already been demonstrated in similar systems. In particular, Issadore *et al*. showed that a 300% increase in magnetic nanoparticle (MNP) loading onto human cancer cells was achieved by using multiple MNPs conjugated to a 1,2,4,5-tetrazine (Tz) onto a scaffold of antibody-conjugated *trans*-cyclooctene (TCO)[7]. The same approach is compatible with magnetic detection using the quantum diamond microscope. Since the ~200-nT magnetic resolution demonstrated in the present work is an order of magnitude finer than that achieved by Issadore, such enhanced MNP-labeling would yield a dramatic SNR improvement.

Implementing the improvements described above would enable much more rapid magnetic imaging, with accessible time scales determined by the strength of the magnetic signal. For example, the same magnetic sensitivity demonstrated in the present work in one minute could be achieved in approximately 200 ms using an appropriate imaging FOV and high frame speed camera. Stronger signals, such as those produced by features closer to the diamond, may be resolved faster with coarser magnetic precision.

As described previously (**Supplementary Note 1**), choosing a higher-resolution objective can also enable intracellular dynamics to be imaged if the associated structures can be suitably labeled magnetically. In addition, the quantum diamond microscope is compatible with cell sorting, as it is nondestructive and localizes target cells. We expect that the combination of sensitivity enhancements and boosted labeling strength would allow for target identification within 10 ms for a similarly large FOV, or more rapidly with a reduced FOV. Faster sorting can further be achieved through parallel sorting channels spread over the large imaging area.

References

1. Jackson, John David. *Classical Electrodynamics*. 3rd ed. New York: Wiley, 1998. Section 5.10.
2. Le Sage, D. *et. al.* Optical magnetic imaging of living cells. *Nature* **496**, 486-489 (2013).
3. Maurer, P.C. *et. al.* Far-field optical imaging and manipulation of individual spins with nanoscale resolution. *Nature Physics* **6**, 912 (2010).
4. Ohno, K., *et. al.* Engineering shallow spins in diamond with nitrogen delta-doping. *Applied Physics Letters* **101**, 082413 (2012).
5. Pezzagna, S., B. Naydenov, F. Jelezko, J. Wrachtrup, and J. Meijer. "Creation efficiency of nitrogen-vacancy centres in diamond." *New Journal of Physics* **12**, 065017 (2010).
6. Naydenov, B. *et. al.* Enhanced generation of single optically active spins in diamond by ion implantation. *Applied Physics Letters* **96**, 163108 (2010).
7. Issadore, D. *et. al.* Ultrasensitive clinical enumeration of rare cells ex vivo using a μ-Hall detector. *Science Translational Medicine* **4**, 141ra92 (2012).